JOURNAL OF THERMOPHYSICS AND HEAT TRANSFER
Vol. 9, No. 1, January–March 1995

Transient Compressible Flow and Heat Transfer Within a Heterogeneous Porous System

A. Bouhouch,* M. Prat,† and S. Bories†
Institut de Mécanique des Fluides de Toulouse, 31400 Toulouse, France

This article presents a model for the study of compressible flow and heat transfer within a heterogeneous porous system undergoing a depressurization or repressurization process. The model is used to investigate the flow and the heat transfer phenomena in the external thermal protection system of a hypersonic plane during the launch and re-entry phases. Simulations are carried out for various system and flow conditions. The low-pressure effects on the permeability and the porous medium thermal conductivity are taken into account in the model.

Nomenclature

D_k = low-pressure effect coefficient
D_{slip} = low-pressure effect coefficient
d = pore length scale
Kn = Knudsen number
k = apparent permeability
k_0 = intrinsic permeability
L = macroscopic length scale
M = fluid molecular weight
P = pressure
$(\rho C_p)^f$ = fluid specific heat
$(\rho C_p)^*$ = porous medium specific heat
R = gas constant
r = R/M
T = temperature
t = time
U = filtration velocity
V = intrinsic phase average velocity modulus, $\varepsilon^{-1}\sqrt{U_x^2 + U_y^2}$
x = spatial coordinate
y = spatial coordinate
δ = gas molecule mean free path
ε = porosity
λ^* = porous medium thermal conductivity
μ = dynamic viscosity
ν = kinematic viscosity
ρ = fluid density

I. Introduction

THE development of a new technology such as the design of a Space Shuttle or a hypersonic plane is connected to a great variety of problems. We focus on the flow and heat transfer problems within a composite system that can be considered as a representative example of the main zone of the external thermal protection system of a hypersonic space vehicle. As can be seen from Fig. 1, this thermal protection is based on a system of thin ceramic nonporous tiles and two high-porosity fibrous insulators. The two fibrous insulators are internal multiscreen insulation (IMI), and semi-rigid insulation (SRI), respectively. Note also the presence of high-porosity fibrous seals between the tiles. Because of the rapid changes in the external pressure, depressurization and repressurization phenomena occur within the space under the shingle during the launch and re-entry phases. Therefore, during these phases, there exists a pressure difference between the internal and the external side of a shingle. This pressure difference should not lead to excessive loads on the shingle. Typically, the pressure difference should not exceed 10 mbar for the specific system we have studied. Furthermore, heat transfer by convection is generated by the flow induced by the pressure gradients within the space under the shingle. Therefore, in addition to the load constraint on the shingle, the system should also be designed to limit the overheating of the cold structure (which is metallic and nonporous), associated with the forced convection phenomena. For the specific system considered in the present study, the maximum cold structure temperature should not exceed 170°C. Under these circumstances, the purpose of this article is to present a model for the analysis of the aforementioned problems and to provide representative results of numerical simulations based on this model.

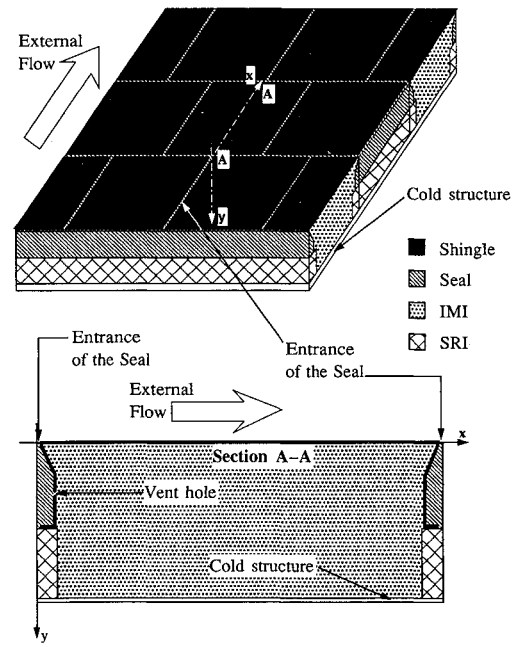

Fig. 1 Overall picture of the system and schematic section of the volume under an elementary shingle. The seals, the IMI, and the SRI are high-porosity fibrous materials. The shingle and the cold structure are nonporous.

Received July 19, 1993; revision received May 17, 1994; accepted for publication May 18, 1994.

*Graduate Student, Institut National Polytechnique, U.R.A. C.N.R.S. no. 0005, Avenue du Professeur Camille Soula.

†Research Scientist, Centre National de la Recherche Scientifique, Institut National Polytechnique, U.R.A. C.N.R.S. no. 0005, Avenue du Professeur Camille Soula.

II. Flow and Heat Transfer Model

The problem definition makes clear that we are faced with a nonconventional problem in terms of transport phenomena in porous medium: First, the density of the fluid phase changes during the pressurization and depressurization processes because of the pressure and temperature variations. Thus, we have to consider an unsteady variable density flowfield. Second, the temperature variation is very important, at least in the re-entry case. Third, we have to account for very low pressures at the end of the launch phase and during most of the re-entry phase. This fact makes the validity of the continuum approach on which the model is based questionable. The model presented in this article is essentially a partially ad-hoc extension of what is used to describe more conventional situations. No effort was made to derive the present model by means of rigorous methods such as, e.g., volumetric-averaging methods. However, we carefully identified the assumptions and restrictions associated with our model. The objective of this study is to provide a useful tool for analyzing the problem of interest. A study based on numerical simulations at the microscale and results drawn from an averaging technique is being undertaken in parallel to define the domain of validity of the macroscopic model. This study will be the subject of a forthcoming paper. In essence, the present model is a combination of Darcy's law with the ideal gas law, together with an energy equation based on the local thermal equilibrium assumption. Assuming isotropic, homogeneous, and nondeformable materials, the considered macroscopic equations are

Mass of the fluid phase

$$\varepsilon \frac{\partial \rho}{\partial t} + \nabla \cdot (\rho U) = 0 \tag{1}$$

Momentum (Darcy's law)

$$U = -(k/\mu)\nabla P \tag{2}$$

Energy

$$(\rho C_p)^* \frac{\partial T}{\partial t} + (\rho C_p)_f U \cdot \nabla T = \nabla \cdot (\lambda^* \nabla T) \tag{3}$$

Ideal gas law

$$P = \rho r T \tag{4}$$

Combining Eq. (2) with Eq. (1) leads to

$$\varepsilon \frac{\partial \rho}{\partial t} + \nabla \cdot \left(-\rho \frac{k}{\mu} \nabla P \right) = 0 \tag{5}$$

Making use of Eq. (4) we express Eq. (5) as

$$\frac{1}{T}\frac{\partial P}{\partial t} = \frac{1}{\varepsilon} \nabla \cdot \left(\frac{Pk}{T\mu} \nabla P \right) + \frac{P}{T^2}\frac{\partial T}{\partial t} \tag{6}$$

Determining the temperature, pressure, and velocity fields for the problem under consideration amounts to solving Eqs. (2), (3), and (6) with appropriate initial and boundary conditions.

At this stage, several remarks are worth being made. First, the problem essentially takes the form of two coupled equations, Eqs. (3) and (6). Equation (6) is a nonlinear diffusion-type equation with source term. Equation (3) is a diffusion-convection-type equation. Thermal dispersion is neglected, i.e., λ^* is the stagnant thermal conductivity of the porous medium. Also, reversible work and viscous dissipation are neglected in the energy equation. Since we deal with high porosity materials, $\varepsilon \approx 0.99$, and high temperatures, radiative heat transfer within the fibrous materials is not negligible. The radiative heat transfer is taken into account through λ^*, which is determined experimentally. The air viscosity as a function of temperature is determined by means of the Sutherland's expression, $\mu = 1.462 \times 10^{-6}[\sqrt{T}/1 + (112/T)]$ $\mathrm{kgm^{-1}s^{-1}}$, with T in Kelvin. Perhaps questionably, we make use of Darcy's law. As it is well known, Darcy's law is, in principle, valid only for very low Reynolds number incompressible steady flows in porous media. Here, we deal with compressible and transient flows. However, as will be discussed later, the Mach number and the Reynolds number of the flow studied herein are indeed very low. This enables us to have confidence in using Darcy's law. In fact, under isothermal conditions, our flow model reduces to the classical model of a slightly compressible flow in a porous medium.[1,2] Derivation of this classical model has been obtained by Aganovic and Mikelic[3] within the framework of the homogenization method. In their analysis of compressible flow and heat transfer in a packed bed, Vafai and Sozen[4,5] used a model similar to the one presented in our study. One interesting difference with our model, however, is the use of a two-phase model for the thermal transfer. This enabled Sozen and Vafai to explore the validity of the local thermal equilibrium assumption. According to their results, the local thermal equilibrium assumption may be carried out for the low Reynolds and Darcy number flows considered in the present study. The processes studied by Sozen and Vafai[4,5] are transient, and this aspect is discussed in Sozen and Vafai.[4,5] However, a central difficulty in the present problem is the strongly transient character of the flow. More work is certainly needed to assess the validity of the present model under strongly transient conditions from a rigorous standpoint.

Let us turn next our attention to the low-pressure problem. Figure 2 shows the time evolution of the local pressure, and the equilibrium temperature at the external surface of the shingle. As can be seen from Fig. 2, low pressures are encountered at the end of the launch phase and during most of the re-entry phase. Clearly, it does not make sense to use a standard continuum approach when the pressure is almost

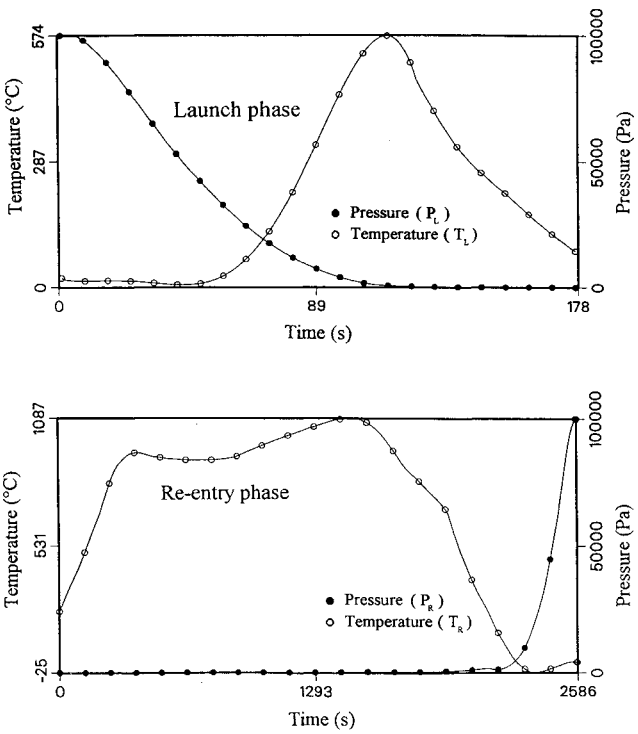

Fig. 2 Evolution of the pressure and the equilibrium temperature at the external side of a shingle in the launch and the re-entry phase.

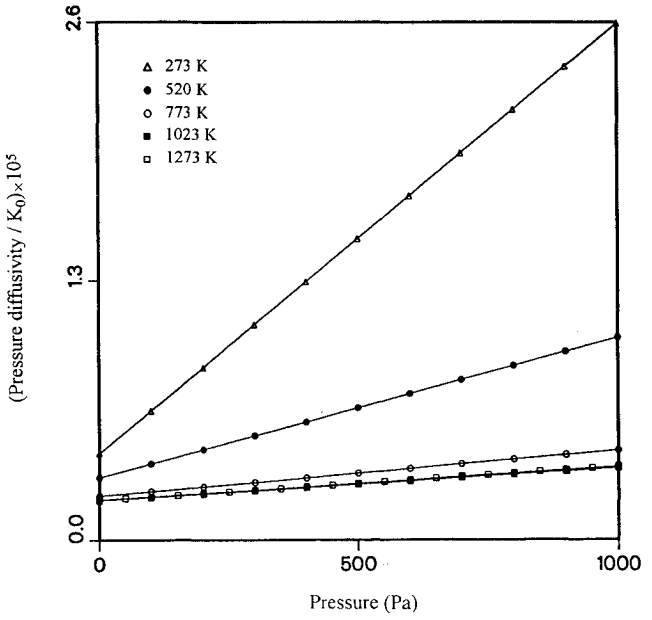

Fig. 3 Pressure diffusivity as a function of pressure and temperature.

Table 1 Intrinsic permeability of each component

$k_{\text{cold structure}}$, m^2	k_{tile}, m^2	k_{seal}, m^2	k_{ISR}, m^2	k_{IMI}, m^2
0.0	0.0	2.3×10^{-10}	10^{-11}	2.4×10^{-9}

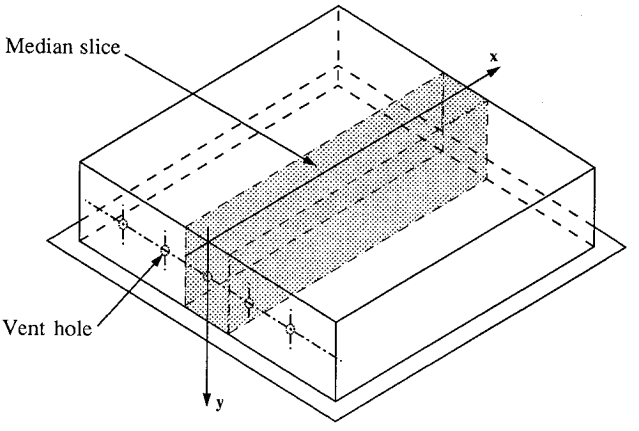

Fig. 4 Three-dimensional schematic diagram of a tile.

zero. However, low-pressure gas flows in porous media have been studied and it has been shown that a slip phenomenon at the wall should be taken into account.[6] According to Klinkenberg,[7] this effect can be taken into account by considering an apparent permeability that is a function of the ratio of the mean free path of the gas molecules to the typical size of the pores. In fact, the correction term can be expressed in terms of pressure and temperature (see Appendix). Under these circumstances, as explained in the Appendix, the "diffusion" coefficient in Eq. (6), i.e., $(Pk/T\mu\varepsilon)$, approaches a limit different from zero when the pressure tends to zero. In Fig. 3, the evolution of $(Pk/T\mu\varepsilon)/k_0$ as a function of P and T is plotted. Here, k_0 is the permeability corresponding to a pure viscous flow, i.e., when the low-pressure slip effect is negligible.

Influence of the gas pressure on the effective thermal conductivity of porous media has also been reported.[8] In the case of sands, Hahne et al. found a very significant reduction of the effective thermal conductivity when the gas pressure decreases. This can be explained in terms of the gas kinetic theory. Clearly, when the gas pressure tends to zero, conductive heat transfer from one grain to another occurs only through the point of contact between the grains. This corresponds to a lower limit for the effective thermal conductivity. In the case of fibrous materials of high porosity, similar effects are observed. In the present study, values of the thermal conductivity of each material as a function of pressure are obtained by interpolation from the measured values at 0.01, 0.1, 1, 25, and 1000 mbar. These data have been obtained by Dassaults.[9]

III. Simulations and Discussion of Results

Equations (3) and (6) are solved by means of a two-dimensional finite element method. We use a Galerkin weighted residual method with rectangular elements. As relatively high mesh Peclet numbers cannot be avoided during the launch phase, care must be exercised for the numerical treatment of Eq. (3). Upwinding of the convective term is obtained through the Petrov-Galerkin weighted residual formulation developed by Brooks and Hughes.[10] A 45 × 60 node mesh is used.

Figure 4 shows a schematic three-dimensional view of the tile. Clearly, a detailed determination of what happens in the system under investigation would require three-dimensional computations. Note also that the presence of five vent holes drilled through one of the tile flanks prevents from fully taking advantage of the apparent symmetries of the domain. However, we believe that much insight can be gained through two-dimensional computations, provided that some precautions are taken in order to take into account the vent holes. In particular, the crossing area-volume ratios should be respected. In fact, the results presented in what follows are viewed as accounting for the transfers within the median slice sketched in Fig. 4. To satisfy the vent hole crossing area-volume ratio, a slot smaller than the vent hole diameter is considered for the two-dimensional simulations. For instance, a 0.4-mm-wide slot corresponds to a 5-mm-diam vent hole. The values of the permeabilities for each component of the system are given in Table 1. The thermal properties and the permeability assigned to the finite elements representing the vent hole are those of the IMI.

A. Launch Phase

As boundary conditions, the pressure at the entrance of the seals and the temperature on the external side of the tile are specified according to the curves depicted in Fig. 2 (i.e., $P = P_L$, $T = T_L$ at $y = 0$ $\forall x$). Zero flux conditions are imposed at the remaining boundaries of the domain, including at the boundary of the cold structure. Initially, the pressure and the temperature within the space under the shingle are uniform and respectively equal to the atmospheric pressure and 21°C.

Figure 5 shows a representative pressure field within the volume under the shingle. As can be seen from Fig. 5, the pressure gradients are high within the seals and the SRI that act as pressure barriers. In the IMI region, the pressure is quasiuniform and the flow is essentially parallel to the external edge of the tile. The temperature field at the same time is depicted in Fig. 6. A fin effect associated with the relatively greater thermal diffusivity of the tile is clearly evidenced along the tile flanks. The evolution of the maximum pressure difference between the internal and external sides of the tile as a function of time is shown in Fig. 7. The pressure difference, defined as $\max(P_{\text{internal side}} - P_{\text{external side}})$, is maximum at about 100 s after takeoff. This corresponds to a slope change in the pressure curve depicted in Fig. 2.

In order to identify the most important features of the model and of the system under investigation, a sensitivity analysis has been carried out. In terms of the model, the influence of the source term in Eq. (6), the convective term in Eq. (3), the permeability, and the thermal conductivity low-pressure corrections has been investigated. In terms of

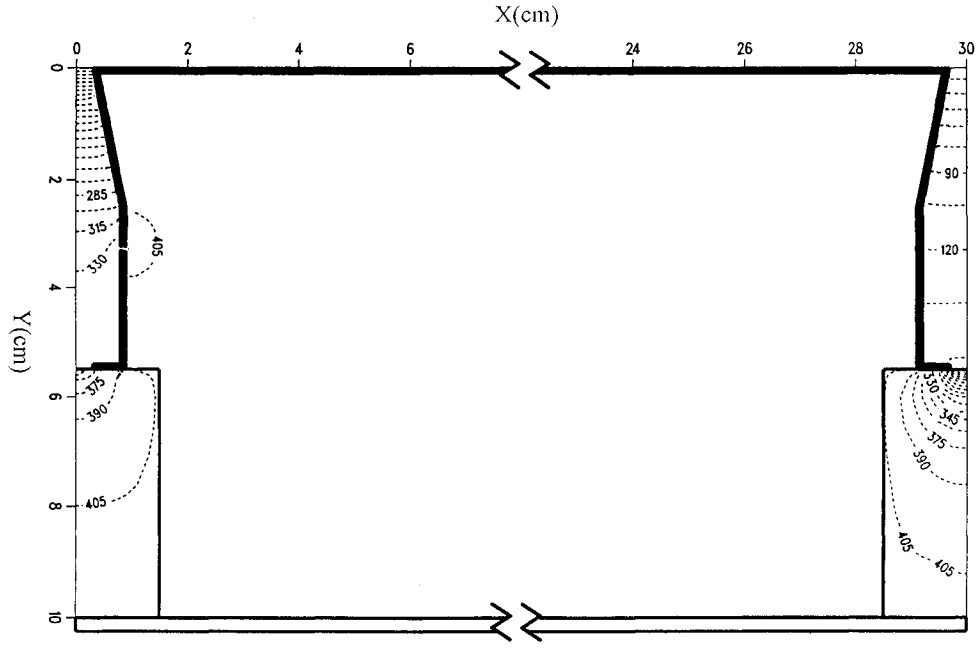

Fig. 5 Example of the pressure field within the under shingle volume in launch phase (time = 176 s, external pressure = 1 Pa, minimum internal pressure = 408 Pa, pressure increment = 15 Pa).

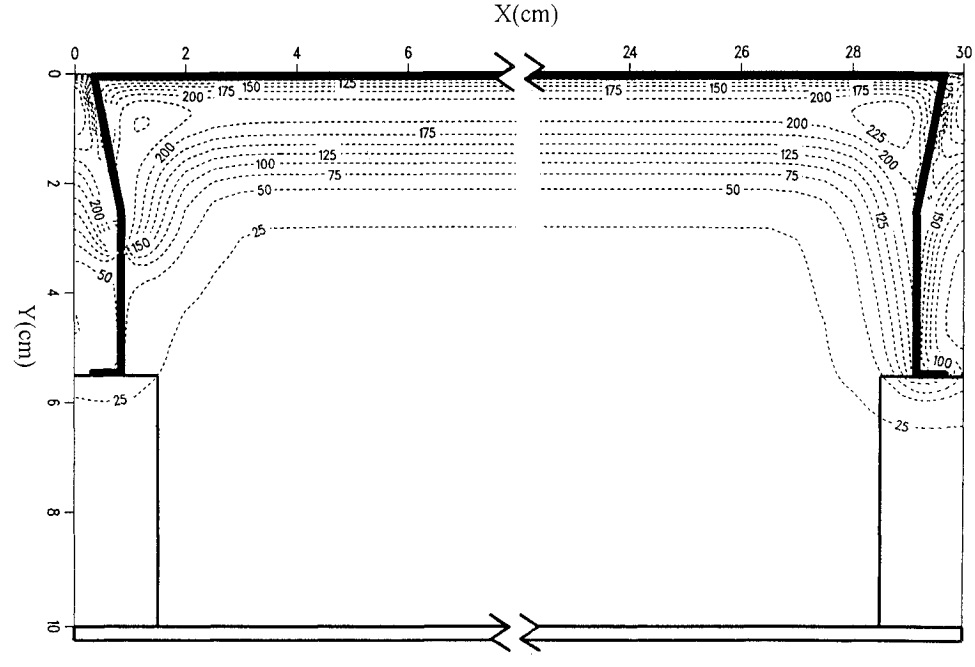

Fig. 6 Example of the temperature field within the under shingle volume in launch phase (time = 176 s, external temperature = 82°C, minimum internal temperature = 21°C, temperature increment = 25°C).

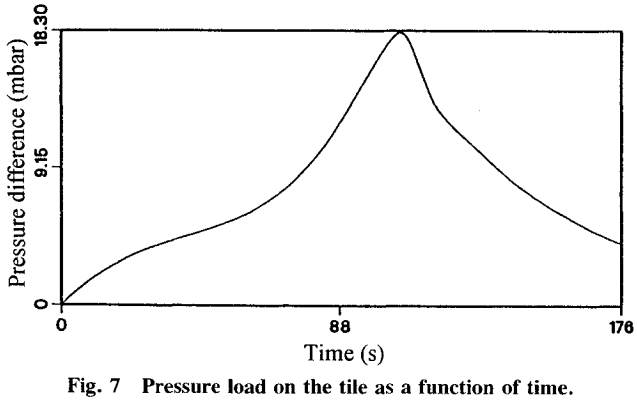

Fig. 7 Pressure load on the tile as a function of time.

the system, the effect of the vent holes and the seal permeability has been studied. Results are summarized in Table 2.

As can be seen from Table 2, vent holes are useful to limit the pressure load on the shingle. The role of the vent hole is exemplified in Fig. 8, which shows the mass flow rates at various locations as a function of time. In the absence of vent holes, emptying of the IMI region occurs through the SRI, which are low permeability regions. The seal permeability is also a sensitive parameter. This is consistent with the structure of the flow shown in Fig. 5, since the high-pressure gradients are located in the seals. In terms of the model, the influence of the low-pressure effects is not negligible. Here, the low-pressure effects contribute to reduce the load on the shingle since the low-pressure slip effect tends to reduce the apparent permeability. One can also see that the source term in Eq.

(6) associated with the temperature variations may be neglected. In terms of the system, the maximum pressure difference is about twice the 10 mbar technically required maximum constraint in the most favorable case. However, a 20-mbar pressure load can still be considered as reasonable, the 10-mbar constraint indicating only an order of magnitude of the acceptable pressure constraint.

Table 2 Sensitivity analysis, launch phase

	Maximum pressure difference, mbar
Full model, base configuration	18.3
$k_{seal} = k_{seal}/2.3$	32.04
No vent hole	27.29
No low-pressure correction on k and λ^*	20.91
$\frac{P}{T^2}\frac{\partial T}{\partial t}$ neglected in Eq. (6)	18.9

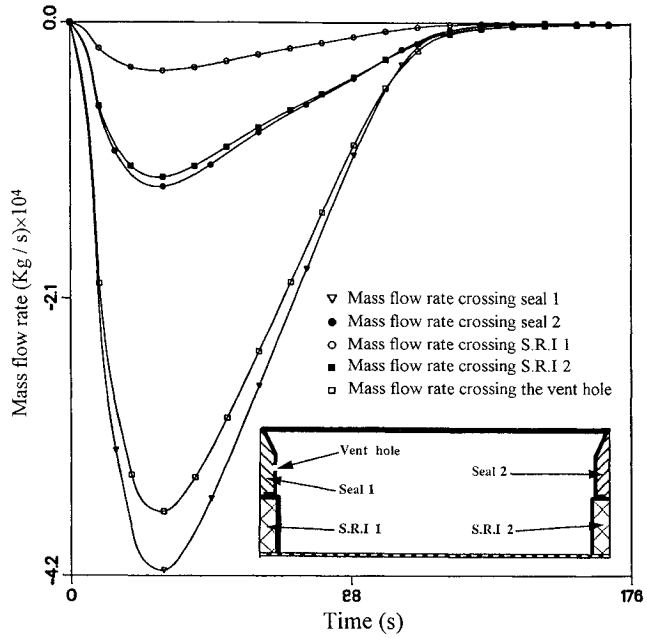

Fig. 8 Time evolution of the mass flow rates at various locations within the under shingle volume during the launch phase.

B. Re-Entry Phase

With reference to the re-entry phase, the main issue is to evaluate the influence of the forced convection associated with the progressive repressurization of the volume under the shingle on the warming up of the cold structure. The boundary conditions expressed in terms of the local pressure and the equilibrium temperature at the surface of a tile are shown in Fig. 2 (i.e., $P = P_R$, $T = T_R$ at $y = 0$ $\forall x$). They correspond to the re-entry trajectory that is critical regarding the cold structure overheating problem. Zero flux conditions are imposed at the remaining boundaries of the computational domain. Initially, the temperature distribution within the system corresponds to the steady conductive process obtained for $T = 130$°C on the external side of the tile, and $T = 45$°C on the cold structure. This is the temperature distribution obtained when the space vehicle is warmed up by the solar radiation. Also, at the initial stage, the pressure is zero within the domain of interest.

Figure 9 shows a typical pressure field. The flow and pressure fields present the same basic structure as for the launch phase, i.e., high-pressure gradients within the seals and the SRI, and quasiuniform pressure within the IMI. Temperature fields at various times are shown in Fig. 10. The fin effect observed during the launch phase is only observed at the beginning of the re-entry phase. This can be explained in terms of thermal diffusivity since the discrepancies between the thermal diffusivities of each component tend to decrease with the temperature as can be seen from Fig. 11. The cold structure maximum temperature evolution as a function of time is shown in Fig. 12. The maximum cold structure temperature obtained is 118°C, well below the required 170°C technical constraint. However, it is worth noting that heat conduction through the shingle anchoring clips is not taken into account in the simulations, our main objective being to evaluate the influence of the convective heat transfer.

A sensitivity analysis similar to the one presented for the launch phase has been carried out for the re-entry phase. Results are summarized in Table 3. Based on Table 3, the influence of the forced convection heat transfer is quite weak. From Fig. 2, which shows the time evolution of the boundary conditions, one can see that the external pressure increases significantly towards the end of the re-entry phase. This section of the re-entry phase corresponds to low external temperatures (Fig. 2). The effect of forced convection heat trans-

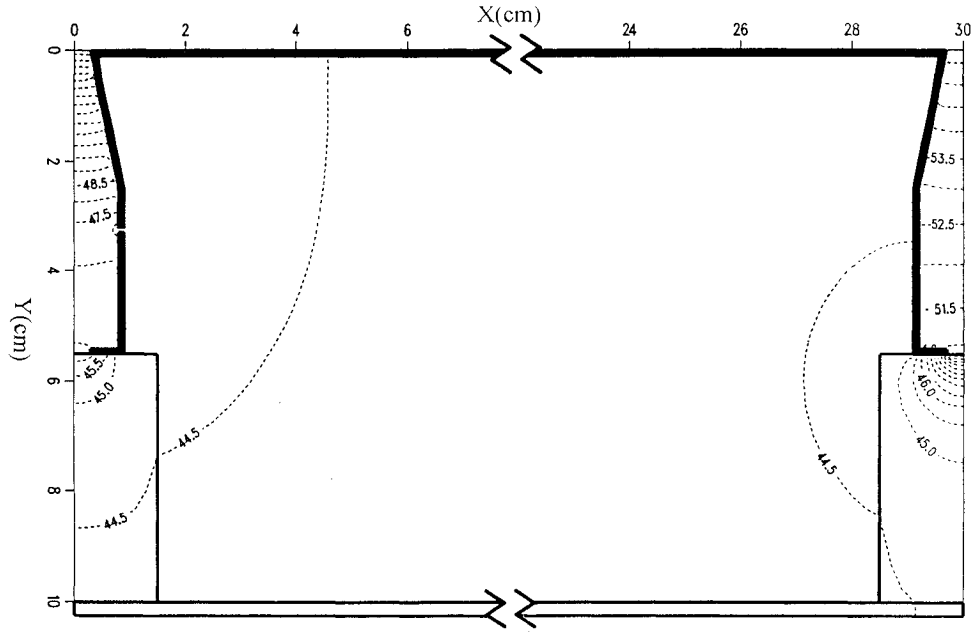

Fig. 9 Example of the pressure field within the under shingle volume in re-entry phase (time = 421 s, external pressure = 56 Pa, minimum internal pressure = 44 Pa, pressure increment = 0.5 Pa).

Table 3 Sensitivity analysis, re-entry phase

	Maximum pressure difference, mbar	Total energy transferred to the cold structure, kJ	Cold structure maximum temperature, °C
Full model, base configuration	−4.46	146.5	117.8
$k_{seal} = k_{seal} \times 2.3$	−2.11	146.7	118.0
No vent hole	−14.67	147.2	118.1
No low-pressure correction on k and λ^*	−4.93	361.8	228.9
Heat transfer by convection neglected	−4.47	146.4	117.6

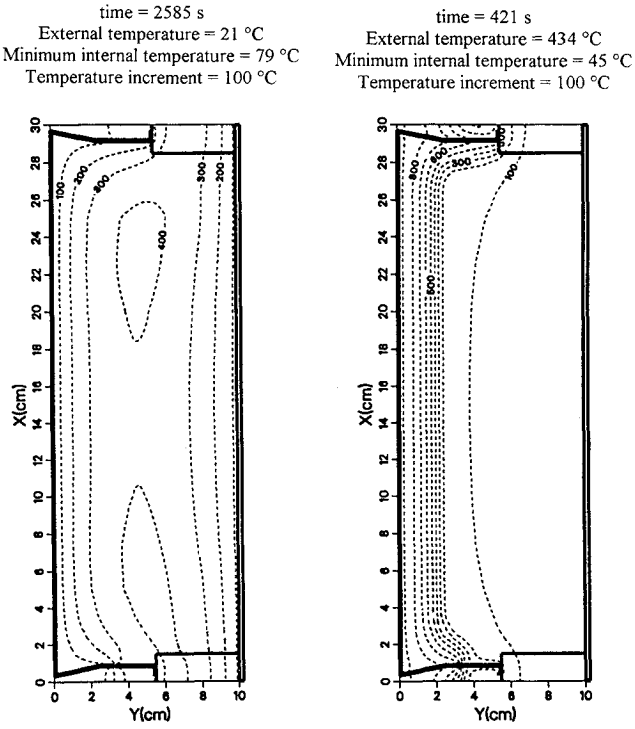

Fig. 10 Temperature fields within the under shingle volume at two stages of the re-entry phase.

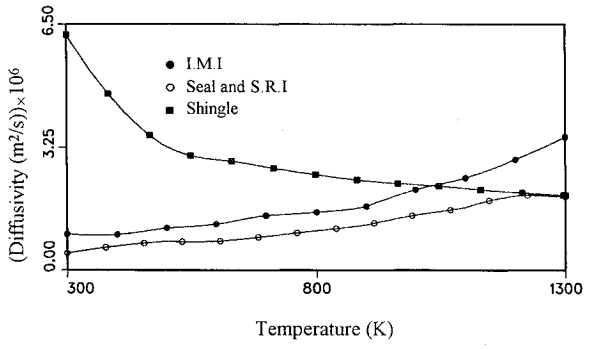

Fig. 11 Thermal diffusivities as a function of temperature at 1000 mbar.

fer would be different if significant pressures were encountered earlier during the re-entry phase. Low-pressure effects are very important owing to the significant reduction of the thermal conductivity in the pressure regime. In terms of the pressure load, the maximum pressure differences defined as $\max(P_{\text{internal side}} - P_{\text{external side}})$ are less than in the launch phase and below the 10 mbar required constraint, except for the no vent hole case.

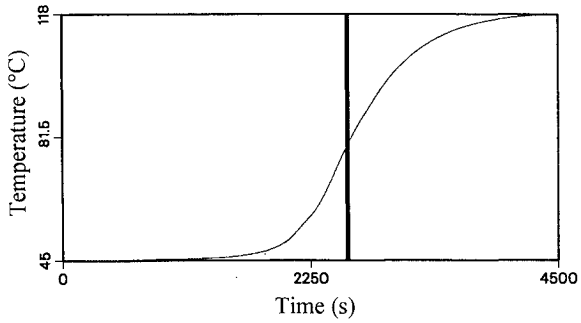

Fig. 12 Cold structure maximum temperature vs time.

IV. Conclusions and Model Validity

The compressible flow model used herein is based on Darcy's law that is, in principle, only valid for steady incompressible flows at very low Reynolds number. In the present study, however, we deal with variable density transient flows. A pore level Reynolds number can be estimated as $Re = (V\sqrt{k_0}/\nu)$. The maximum Reynolds number is observed within the vent hole during the launch phase. As can be seen from Fig. 13, the maximum Reynolds number is always smaller than 2.2. The Mach number can be estimated as $Ma = (V/c)$, in which c denotes the sound speed, $c = \sqrt{\gamma rT}$, with $\gamma = 1.4$ for an ideal gas, and $r = 287$ J/kg K for air. T is the air temperature. This leads to Mach numbers no greater than 0.01. Therefore, in terms of Mach and Reynolds numbers, the results are consistent with Darcy's law. Regarding the issue of transient flow, to estimate the transient character of the flow, one can compare the two following time scales:

1) $t_v = (d^2\rho/\mu)$, where the quantity t_v is the time scale associated with a transient viscous flow at the pore level. As $k_0 \approx d^2$, t_v can be expressed in terms of permeability as $t_v = (k_0\rho/\mu)$.

2) $t_p = (L^2\mu\varepsilon/Pk_0)$ where the quantity t_p is the pressure diffusion time scale. Then, $(t_v/t_p) = (k_0^2/L^2)P^2\mu^{-2}(1/\varepsilon rT)$. With $l \approx 0.1$ m, (t_v/t_p) is in the range 0.1–1.

As the two aforementioned time scales might be of the same order of magnitude, it should be concluded that transient effects might be significant. Further study is certainly needed to assess the relevance of Darcy's law under these circumstances. Nevertheless, except perhaps for very particular circumstances associated with strongly transient flows, the model presented in this article allows us to compute the flow and the heat transfer within a heterogeneous porous system that undergoes depressurization or repressurization phenomena under nonisothermal conditions. In terms of the specific system that has been studied, the simulations have shown 1) the significant influence of the seal permeability on the shingle pressure load, 2) the influence of the vent holes that contribute markedly to reduce the pressure load on the shingle, 3) the negligible effect of the forced convection heat transfer, and 4) the strong influence of the low-pressure effect on the thermal transfer owing to the significant reduction of the thermal conductivity with the low pressures.

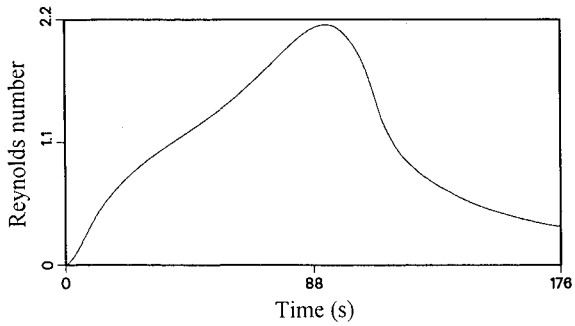

Fig. 13 Maximum Reynolds number as a function of time during the launch phase.

These results have been obtained by means of two-dimensional simulations. More accurate results would probably be obtained with three-dimensional computations. However, on the basis of the pressure and temperature fields obtained with the two-dimensional simulations, it appears that three-dimensional simulations are not required to determine the shingle pressure load and to assess the influence of the heat transfer by convection that were our main objectives.

Appendix: Low-Pressure Flow in Gas

In this Appendix, modeling of gas flow at low pressure is presented. What follows borrows heavily from Kaviany.[11] At low pressure, the mean free path of gas molecules is no longer much smaller than the pore size. Under these circumstances, flow behavior deviates from pure viscous flow behavior and a greater flow rate than that expected for purely viscous flow is generally observed. This deviation is associated with a molecular slip effect at the fluid solid interface. A useful parameter to characterize this phenomenon is the Knudsen number that is

$$Kn = (\delta/d) \tag{A1}$$

Thus, viscous flows correspond to $Kn \ll 1$. δ is given as

$$\delta = (k_b T/2^{5/2}\pi R_m^2 P) \tag{A2}$$

where k_b is the Boltzmann constant, $k_b = 1.381 \times 10^{-23}$ (J/K). R_m is the collision cross section radius, $R_m = 3.61/2$ Å for air.

In terms of the mass flow rate, a semiempirical relation for accounting for the Knudsen effect is given by Weber[11] as

$$\rho U_x = -\frac{k_0}{\mu}\frac{P}{RT}\frac{dP}{dx} - \frac{4}{3}\left(1 - \frac{Kn}{1+Kn}\right) D_{slip}\frac{1}{RT}\frac{dP}{dx} - \frac{Kn}{1+Kn} D_k \frac{1}{RT}\frac{dP}{dx} \tag{A3}$$

where D_{slip} and D_k are determined by means of the kinetic theory. k_0 corresponds to the purely viscous case.

D_k is given as (Ref. 11, p. 341)

$$D_k = C_k\sqrt{RT} \tag{A4}$$

where C_k depends on the matrix structure and is determined experimentally. In the absence of available data for fibrous materials, we assumed that $C_k = 7 \times 10^{-7}$ m, which is the sole value quoted by Kaviany,[11] and corresponds in fact to a fritted glass filter.

In the case of a tube flow D_{slip} is given as

$$D_{slip} = (\pi r \bar{u}_m/8) \tag{A5}$$

where r is the tube radius, and $\bar{u}_m$ is the mean molecular speed of the gas given as

$$\bar{u}_m = \sqrt{(8RT/\pi)} \tag{A6}$$

Here again, in the absence of representative data for fibrous materials, we have made use of Eq. (A5).

At this stage, we are in a position to, at least qualitatively, evaluate the low-pressure effect on the apparent permeability. From Eq. (A3) we deduce that

$$k = \left\{k_0 + \left[\frac{4}{3}\left(1 - \frac{Kn}{1+Kn}\right)\mu D_{slip} + \frac{Kn}{1+Kn}\mu D_k\right]\frac{1}{P}\right\} \tag{A7}$$

Thus, for given P and T, Kn is determined by means of Eqs. (A2) and (A1), in which d is estimated as $\sqrt{k_0}$. D_{slip} is determined by Eqs. (A5) and (A6), D_k by Eq. (A4), and k by Eq. (A7).

Acknowledgments

Financial support from CNES (Centre National d'Etudes Spatiales), Toulouse, France, is gratefully acknowledged. Special thanks are due to T. Maciaszek and E. Werling for valuable discussions and D. Poulikakos for improving the article.

References

[1]Muskat, M., "The Flow of Homogeneous Fluids Through Porous Media," J. W. Edwards, Ann Arbor, MI, 1946.

[2]Bear, J., "Dynamics of Fluid in Porous Media," Elsevier, New York, 1972.

[3]Aganovic, I., and Mikelic, A., "Justification of Viscous Fluid Flow Models in Porous Media," *Heat and Mass Transfer in Porous Media*, edited by M. Quintard and M. Todorovic, Elsevier, Amsterdam, 1992.

[4]Vafai, K., and Sozen, M., "Analysis of Energy and Momentum Transport for Fluid Flow Through a Porous Bed," *Journal of Heat Transfer*, Vol. 112, 1990, pp. 690–699.

[5]Sozen, M., and Vafai, K., "Analysis of Oscillating Compressible Flow Through a Packed Bed," *International Journal of Heat and Fluid Flow*, Vol. 12, No. 2, 1991, pp. 130–136.

[6]Dullien, F. A. L., "Porous Media Fluid Transport and Pore Structure," Academic Press, San Diego, CA, 1992.

[7]Klinkenberg, M., "The Permeabilities of Porous Media to Liquids and Gases," *Amer. Petrol. Inst. Drilling Prod. Pract.*, 1941, pp. 200–213.

[8]Hahne, H., Strong, Y. W., and Gross, U., "Measurement of Thermal Conductivity in Porous Media," NATO Advanced Study Inst. on Convective Heat and Mass Transfer in Porous Media, Izmir, Turkey, 1990, pp. 523–539.

[9]Paret, A., and Illouz, J., Dassault Co., TR H-SG-1BF-1001-AMD, Toulouse, France, 1991.

[10]Brooks, A. N., and Hughes T., "Streamline Upwind Petrov-Galerkin Formulations for Convection Dominated Flows with Particular Emphasis on the Incompressible Navier-Stokes Equations," *Computer's Methods in Applied Mechanics and Engineering*, Vol. 32, 1982, pp. 199–259.

[11]Kaviany, M., *Principles of Heat Transfer in Porous Media*, Springer-Verlag, North-Holland, Amsterdam, 1991.